CORE
Metadata, citation and similar papers at core.ac.uk
Provided by Explore Bristol Research

Huang, G., Nix, A. R., & Armour, S. M. D. (2007). Impact of radio resource allocation and pulse shaping on PAPR of SC-FDMA signals. In IEEE 18th International Symposium on Personal, Indoor and Mobile Radio Communications, 2007 (PIMRC 2007), Athens. (pp. 1 - 5). Institute of Electrical and Electronics Engineers (IEEE). 10.1109/PIMRC.2007.4394297

Link to published version (if available):
10.1109/PIMRC.2007.4394297

Link to publication record in Explore Bristol Research
PDF-document

University of Bristol - Explore Bristol Research

General rights

This document is made available in accordance with publisher policies. Please cite only the published version using the reference above. Full terms of use are available:
http://www.bristol.ac.uk/pure/about/ebr-terms.html

Take down policy

Explore Bristol Research is a digital archive and the intention is that deposited content should not be removed. However, if you believe that this version of the work breaches copyright law please contact open-access@bristol.ac.uk and include the following information in your message:

• Your contact details
• Bibliographic details for the item, including a URL
• An outline of the nature of the complaint

On receipt of your message the Open Access Team will immediately investigate your claim, make an initial judgement of the validity of the claim and, where appropriate, withdraw the item in question from public view.

The 18th Annual IEEE International Symposium on Personal, Indoor and Mobile Radio Communications (PIMRC'07)

IMPACT OF RADIO RESOURCE ALLOCATION AND PULSE SHAPING ON PAPR OF SC-FDMA SIGNALS

Gillian Huang, Andrew Nix and Simon Armour
Centre for Communications Research, University of Bristol
Merchant Venturers Building, Woodland Road, Bristol BS8 1UB, UK
Email: G.Huang@bristol.ac.uk

ABSTRACT

"Single Carrier Frequency Division Multiple Access" (SC-FDMA) is a strong candidate for uplink transmissions in the 3G Long Term Evolution (LTE) standard. SC-FDMA is a multiple access scheme that uses DFT spreading prior to OFDM modulation to map the signal from each user to a subset of the available subcarriers. SC-FDMA has a significantly lower peak-to-average power ratio (PAPR) compared to OFDM/OFDMA. This greatly improves its RF power amplifier efficiency and also the mean power output from a battery driven mobile terminal. In this paper, the impact of radio resource allocation and pulse shaping on the PAPR of SC-FDMA signals are investigated, especially for localized FDMA (LFDMA) signals. It is shown that distributed FDMA (DFDMA) signals with raised cosine filtering experience reduced PAPR as α increases. However, for LFDMA signals the PAPR increases with increasing α and further varies according to the allocated resource unit.

I. INTRODUCTION

Broadband wireless communication systems must achieve high data rates in a spectrally efficiency manner. For this reason, Orthogonal Frequency Division Multiplexing (OFDM) [1,2] has been widely employed in systems such as the IEEE 802.11a/g standards. Orthogonal Frequency Division Multiple Access (OFDMA) is a multiple access scheme for OFDM that works by assigning each user a unique set of subcarriers. OFDMA is currently employed in the IEEE 802.16 standard. One major drawback of OFDM and OFDMA is the high peak-to-average power ratio (PAPR) that results from a multicarrier signal [2]. High-PAPR transmit signals require significant back-off in the power amplifier and this reduces their power efficiency and mean power output. This can be problematic – particularly on the uplink where battery powered terminals struggle to match the data rate and range of the downlink.

3G Long-Term Evolution (LTE) is standardized by the Third Generation Partnership Project (3GPP) and is an evolution to existing 3G technology in order to meet projected customer needs over the next 10-15 years. 3GPP2 is developing CDMA2000 1x Evolution Data-Optimized (1xEV-DO) Revision C as its 3G long term evolution. These standards, along with IEEE 802.16e (Mobile-WiMAX) and IEEE 802.20 (Mobile Broadband Wireless Access), provide a route to 4G technology that supports high mobile data rates.

In order to solve the high PAPR problem seen in the uplink of OFDM/OFDMA, research is now addressing techniques such as a Single-Carrier with Frequency Domain Equalization (SC-FDE). It was proposed in [3] to use OFDM on the downlink and SC-FDE on the uplink. Similarly, the 3G LTE standard uses OFDMA on the downlink and SC-FDMA on the uplink [4]. SC-FDMA has significantly lower PAPR than OFDMA and therefore can greatly improve the power efficiency, operating range or data rate of the mobile terminals. The base station can tolerate high power consumption and greater signal processing complexity.

Interleaved Frequency Division Multiple Access (IFDMA) was proposed in [5]. This approach can be viewed as a single carrier system with the ability to achieve multiple-access in the frequency domain, where each user shares the spectrum using a different set of equi-distant subcarriers spaced across the spectrum. Each user has a unique phase vector to multiply with the transmit signal so the equi-distant subcarrier mapping is performed in the time domain. IFDMA is very similar to distributed FDMA (DFDMA). The difference is that IFDMA signals are generated in the time domain whilst DFDMA signals are generated in the frequency domain.

SC-FDMA (or DFT-spread OFDM) is used in the context of the 3G LTE standard [4]. Here the term "spread" refers to subcarrier allocation for the multiple users. This technique is referred to as OFDM-FDMA with DFT spreading in [6,7]. Only distributed subcarrier mapping was considered in [6,7] since it results in a PAPR that is as low as conventional single-carrier systems. In the 3G LTE standard, both distributed FDMA (DFDMA) and localized FDMA (LFDMA) are under consideration [4]. Each subcarrier mapping scheme has its own strengths and weaknesses. For example, a FDMA system with localized subcarrier mapping is more robust to multiple access interference [8], but DFDMA has a lower PAPR. More importantly, DFDMA is more sensitive to timing and frequency error. Overall, LFDMA still offers significant PAPR improvements compared to OFDMA [9]. An overview of SC-FDMA for uplink transmission is given in [10].

Pulse shaping is required for a single-carrier system to bandlimit the transmit signal. We extend the PAPR analysis first reported in [9] for pulse shaped SC-FDMA and further investigate the impact of resource allocation. When raised cosine pulse shaping is applied to DFDMA signals, the PAPR reduces with increasing α and the allocation of radio resource does not affect the PAPR. This paper demonstrates two interesting pulse shaping effects for LFDMA signals: (1) an increase in PAPR with increasing α and (2) a variation in PAPR as a function of resource allocation.

This paper is organized as follows: Section II gives an overview of SC-FDMA and describes the time-domain signals for DFDMA and LFDMA with varying resource unit (RU) allocation. Section III analyzes the simulation results of a PAPR comparison for DFDMA and LFDMA with varying resource unit allocation and raised cosine pulse shaping. Section IV concludes the paper.

1-4244-1144-0/07/$25.00 ©2007 IEEE.

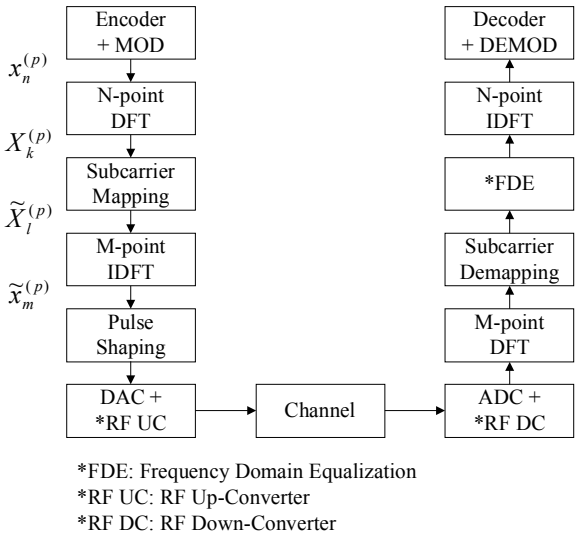

Fig. 1: Baseband system model of SC-FDMA

II. SC-FDMA SYSTEM

A. Overview of SC-FDMA

A baseband system model of SC-FDMA is shown in Fig. 1. The mathematical notation used in this paper follows that reported in [9]. M represents the total number of available subcarriers, where $M = Q.N$. Q denotes the spreading factor and N represents the number of subcarriers assigned to each user. We further assume that each user occupies the same number of subcarriers, so in this case Q also represents the number of users. Each user p, $p = 0,...,Q-1$, generates a block of N complex-valued symbols, $x_n^{(p)}$, $n = 0,...,N-1$. By applying an N-point DFT to $x_n^{(p)}$, the frequency domain symbols $X_k^{(p)}$ can be described as

$$X_k^{(p)} = \sum_{n=0}^{N-1} x_n^{(p)} e^{-j\frac{2\pi}{N}kn} \tag{1}$$

The frequency domain symbols are then mapped onto a set of user-dependent subcarriers. Fig. 2 shows an example of a frequency division multiple-access scheme with distributed and localized subcarrier mapping. There are 16 available subcarriers shared by 4 users and each user occupies 4 subcarriers. Each user must map its frequency domain symbols onto the assigned resource unit (RU) and zeros are inserted for the remaining subcarriers. In DFDMA, the RU for each user is a set of interleaved subcarriers across the available transmission band. DFDMA is robust against frequency selective fading since it better exploits the available frequency diversity [10]. In LFDMA, the RU for each user is a set of adjacent subcarriers. LFDMA can potentially achieve multiuser diversity if for each user the localized section of allocated bandwidth experiences high channel gain. This form of multiuser diversity requires independent frequency selective fading per user combined with intelligent radio resource unit allocation [10].

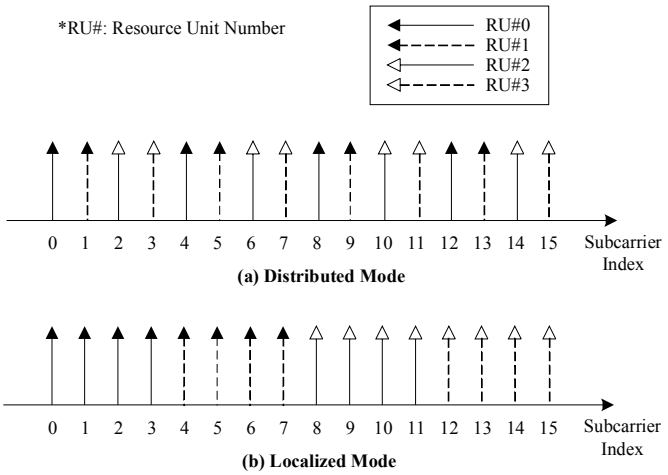

Fig. 2: Multiple access scheme of SC-FDMA:

(a) distributed mode, (b) localized mode.
An example of $M = 16$, $Q = 4$ and $N = 4$.

The frequency domain samples $\widetilde{X}_l^{(p)}$ after the subcarrier mapping process (distributed and localized) are represented by equations (2) and (3) respectively

$$\widetilde{X}_l^{(p)} = \begin{cases} X_k^{(p)} = X_{(l-p)/Q}^{(p)} & , l = Qk + p \\ 0 & , \text{otherwise} \end{cases} \tag{2}$$

$$\widetilde{X}_l^{(p)} = \begin{cases} X_k^{(p)} = X_{l-Np}^{(p)} & , l = k + Np \\ 0 & , \text{otherwise} \end{cases} \tag{3}$$

where l represents the subcarrier index going into the M-point IDFT, $l = 0,...,M-1$ and p is the resource unit number (RU#). It should be noted that p can also denote the user index, i.e. $p = 0,...,Q-1$. After subcarrier mapping, the sampling period $\widetilde{T}$ is reduced, i.e. $\widetilde{T} = (N/M).T$, where T is user input symbol period.

The frequency domain samples $\widetilde{X}_l^{(p)}$ are transformed back into the time domain by an M-point IDFT. The output time domain samples of SC-FDMA before the application of pulse shaping can generally be described as

$$\widetilde{x}_m^{(p)} = \frac{1}{M} \sum_{l=0}^{M-1} \widetilde{X}_l^{(p)} e^{j\frac{2\pi}{M}ml} \tag{4}$$

B. Time-Domain Signal of DFDMA

The derivation of time domain signals for SC-FDMA in [9] is valid when RU#0 is used (see Fig. 2). However, the phase rotations within the SC-FDMA signal are related to the RU being used. Here the RU allocation is taken into account and the method described in [9] is used to derive the SC-FDMA time domain signals. Therefore the DFDMA time domain samples can be obtained by substituting (2) into (1). Let $m = Nq + i$, where $q = 0,...,Q-1$ and $i = 0,...,N-1$. The time domain samples for DFDMA can be described as

$$\tilde{x}_m \left(= \tilde{x}_{Nq+i}\right) = \frac{1}{Q}.e^{j\frac{2\pi}{M}mp}.x_i \qquad (5)$$

where $i = n$, which allows x_i to be written as x_n.

The resulting DFDMA samples $\tilde{x}_m$ are a repetition of the user input symbols x_n, with a phase rotation based on the particular allocation of subcarriers (i.e. RU#). The repetition is determined by the spreading factor, Q. Equation (5) shows that time domain samples are "localized" when the frequency domain samples are interleaved. One simple way to understand the resulting time domain samples in a DFDMA system is to exploit the duality between time and frequency. Upsampling a time domain signal by inserting zeros between the input samples results in frequency spectrum repetition. Hence, by exploiting duality, an interleaved subcarrier mapping scheme should result in sequence repetition of the time domain signal.

Using RU#0 as a reference, the other RU# can be seen as frequency shifted versions of RU#0, as shown in Fig. 2(a). Hence different RU# give different phase rotations in the DFDMA time domain samples, as shown in (5).

C. Time-Domain Signal of LFDMA

The time domain samples for LFDMA can be derived by substituting (3) into (1). Let $m = Qi + q$, where $i = 0,...,N-1$ and $q = 0,...,Q-1$. If $q = 0$, the LFDMA time domain samples can be described as

$$\tilde{x}_m \left(= \tilde{x}_{Qi+q}\right) = \frac{1}{Q}.x_i \qquad (6)$$

where $i = n$, which again allows x_i to be written as x_n. If $q \neq 0$, the LFDMA time domain samples are

$$\tilde{x}_m \left(= \tilde{x}_{Qi+q}\right) = \frac{1}{Q}.e^{j\frac{2\pi}{Q}qp}.\left(1 - e^{j\frac{2\pi}{Q}q}\right).\frac{1}{N}\sum_{n=0}^{N-1}\left\{\frac{x_n}{1 - e^{j\frac{2\pi}{N}\left[(i-n)+\frac{q}{Q}\right]}}\right\} \qquad (7)$$

From (6), the LFDMA time domain samples $\tilde{x}_m$ have exact copies of the input symbols x_n at Q-multiple sample positions, which are independent of the RU# being used. It also shows that time domain samples are "interleaved" when the frequency domain samples are localized. The in-between samples of the LFDMA signal are shown in (7).

Localized subcarrier mapping can be viewed as frequency domain over-sampling. Frequency domain over-sampling can be performed by padding zeros onto unused subcarriers. This results in the interpolation of the input time-domain samples. Similarly, the LFDMA time domain samples $\tilde{x}_m$ are effectively an interpolated version of the input symbols x_n. Given this situation it is possible for the resulting waveform to produce a high output peak. As a result, LFDMA has a higher PAPR than DFDMA without pulse shaping [9].

The summation term in (7) indicates that the in-between samples are strongly correlated with their adjacent input symbols x_n. The first exponential term in (7) represents the phase rotation in the LFDMA time domain samples according to the chosen RU, p. This occurs since the other RU# are frequency shifted versions of RU#0, as shown in Fig. 2(b). It should be noted that phase rotation could make the correlated LFDMA signals more in-phase or out-of-phase depending on the RU#.

D. Pulse Shaping and PAPR

In a single-carrier system, pulse shaping is required to bandlimit the signal and ensures it meets the spectrum mask. Generally speaking, there is a trade-off between spectrum efficiency and PAPR reduction in conventional single-carrier systems [4], but this is not necessarily the case in LFDMA. In this paper, a raised cosine filter is used to pulse shape the SC-FDMA signals.

PAPR is a measure of the peak-to-average power ratio quoted in dB. A transmit signal with high PAPR requires large back-off to ensure the power amplifier operates within its linear region. This reduces the power efficiency of the amplifier and results in a lower mean output power for a given peak power rated device. Hence, a transmit signal with low PAPR is highly desirable for battery powered terminals, where power efficiency is paramount. After pulse shaping, the PAPR of the transmit signal, $x(t)$, can be calculated using the following equation, where $E\{\cdot\}$ denotes the expected value.

$$PAPR = \frac{\max\{|x(t)|^2\}}{E\{|x(t)|^2\}}. \qquad (8)$$

III. Results

The effects of pulse shaping on the PAPR of SC-FDMA signals with different RU# are investigated in this section. In the simulation, the total number of subcarriers M is set to be 512 and each user has access to 64 subcarriers ($N = 64$) with a spreading factor Q of 8. The baseband modulation is QPSK and 100,000 input data blocks are used to calculate the CCDF (Complementary Cumulative Distributed Function) of the PAPR. Time-domain pulse shaping is performed using a raised cosine filter with its impulse response truncated from $-6\tilde{T}$ to $6\tilde{T}$, where $\tilde{T}$ represents the time period of the SC-FDMA time-domain samples, $\tilde{x}_m$. The power of the raised cosine filter is normalized to unity for all α. SC-FDMA signals are over-sampled by 8 times for pulse shaping.

Fig. 3 shows the effects of pulse shaping on the CCDF of the PAPR for DFDMA and LFDMA with RU#0, RU#1, RU#2 and RU#3 respectively. Fig. 3(a) with RU#0 is consistent with the PAPR simulations in Fig. 7(a) of [9]. For DFDMA, the convolution of random samples with the raised cosine filter gives a smaller output peak power with increasing α. The output mean power is always the same when filtering random samples with different α, and hence the PAPR decreases as α increases. The DFDMA time domain samples remain random with a phase rotation that

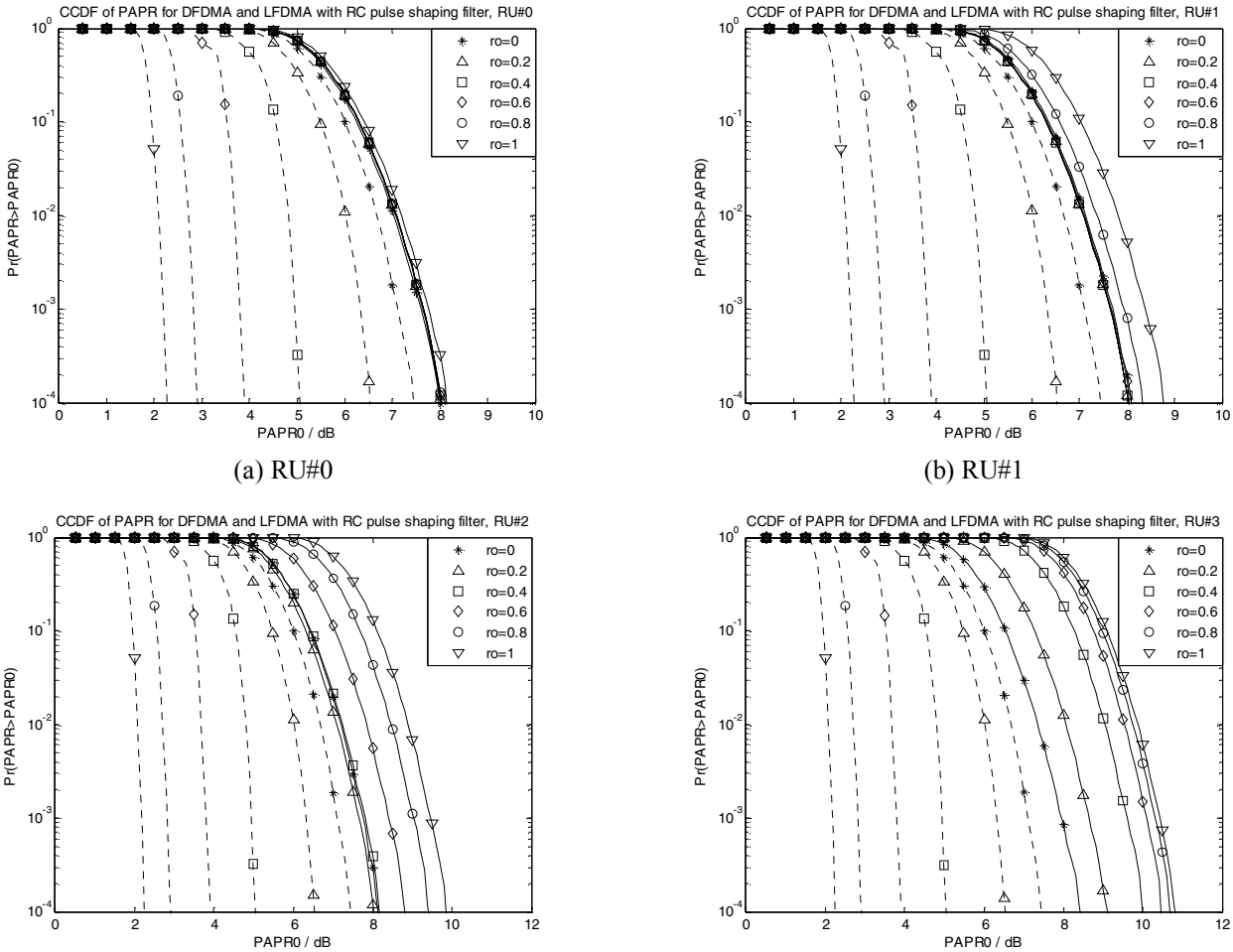

(a) RU#0 (b) RU#1

(c) RU#2 (d) RU#3

Fig. 3: CCDF of PAPR for DFDMA (dashed line) and LFDMA (solid line) signals using raised cosine (RC) pulse shaping filter with α = 0, 0.2, 0.4, 0.6, 0.8 and 1. *ro = rolloff factor, α .

Table 1: Phase rotation of LFDMA in-between samples vs. RU#, *SF: Spreading Factor

Phase rotation	RU#0	RU#1	RU#2	RU#3	RU#4	RU#5	RU#6	RU#7
SF (deg)	22.5	22.5	22.5	22.5	22.5	22.5	22.5	22.5
SF and RU# (deg)	0	45	90	135	180	-135	-90	-45
Total phase rotation (deg)	22.5	67.5	112.5	157.5	-157.5	-112.5	-67.5	-22.5

relates to the choice of RU. As a results, the PAPR of a DFDMA signal does not change with the choice of RU, as shown in Fig. 3.

For pulse shaped LFDMA signals, the PAPR of RU#0, RU#1, RU#2 and RU#3 are the same as the PAPR of RU#7, RU#6, RU#5 and RU#4 respectively. Given this relationship, Fig. 3 is limited to showing the CCDF of the PAPR from RU#0 to RU#3. The link between the PAPR and the RU# arises after pulse shaping because of the phase rotation introduced into the LFDMA in-between samples. Table 1 illustrates that the magnitude of the phase rotation of the LFDMA in-between samples is identical for the RU pairs with matching PAPR. It should be noted that the phase change is inverted between each of these matching pairs. The second row of Table 1 shows the phase rotation due to the spreading factor (SF) Q, which is generated from $1-e^{j\frac{2\pi}{Q}q}$ in (7). The third row shows the phase rotation due to the SF, Q and the RU#, p, i.e. the $e^{j\frac{2\pi}{Q}qp}$ term in (7). Since the total phase rotation of the LFDMA signals are effectively the same, it follows that the PAPR will be identical.

The phase rotation makes the LFDMA samples combine through the pulse shaping filter to be in-phase or out-of-phase, which results in the observed variation of output mean power. Fig. 4 shows the ratio of the output mean power to the input mean power (defined relative to the pulse shaping block) for LFDMA signals with different RU. For RU#0 the LFDMA signal results in a strong in-phase combination (given the phase rotation of 22.5°) after pulse shaping, so the

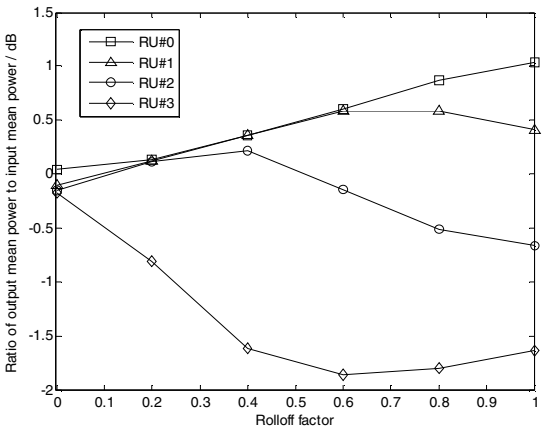

Fig. 4: Ratio of output mean power to input mean power of LFDMA signal with raised cosine pulse shaping

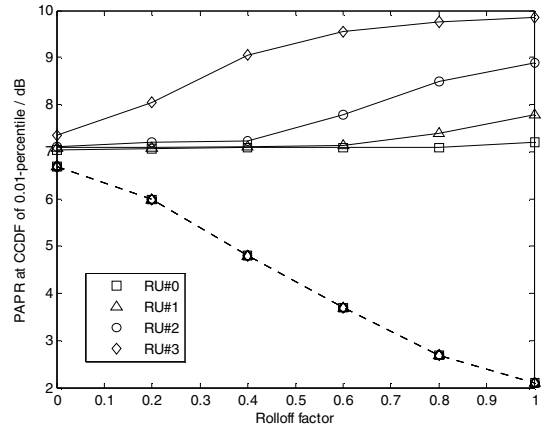

Fig. 5: Comparison of CCDF of PAPR at 0.01-percentile for DFDMA (dashed line) and LFDMA (solid line) signals with raised cosine pulse shaping

output mean power increases. For RU#3, the phase of the LFDMA samples are strongly out-of-phase (phase rotation of157.5°) and hence the output mean power decreases. For the same α , the output mean power shows the following trend RU#0 > RU#1 > RU#2 > RU#3, as shown in Fig. 4.

Due to the phase rotation described earlier, it is unlikely that the LFDMA samples will all add up constructively to produce a high output peak after pulse shaping. From the simulations, the output peak often occurs when the input peak sample convolves with the peak RC filter tap. Since the raised cosine filter power is normalized to unity, the peak power of the raised cosine filter tap becomes larger with larger α . This implies that after pulse shaping the output peak power of the LFDMA signal increases with increasing α .

Fig. 5 shows a comparison of the CCDF of the PAPR at the 0.01-percentile for DFDMA and LFDMA signals with raised cosine pulse shaping. This was produced using the simulation results shown in Fig. 3. It is shown that DFDMA has a lower PAPR than LFDMA when pulse shaping is applied. This is also true without pulse shaping, as mentioned in Section II. For DFDMA, the PAPR is the same for all RU# and the PAPR decreases with increasing α . For LFDMA with RU#0, both the output peak power and the output mean power increase after pulse shaping. Overall, for RU#0 the PAPR barely changes with α . However, when other RU# are selected the resulting PAPR is dominated by the variation in the output mean power after pulse shaping. The PAPR increases when the output mean power decreases (see Fig. 4 and Fig. 5) and as such the PAPR of an LFDMA signal tends to increase with increasing α .

IV. Conclusions

In this paper, the effects of pulse shaping and the choice of RU on the PAPR of SC-FDMA were investigated. SC-FDMA is attractive for uplink transmissions since it reduces the high PAPR seen with OFDM/OFDMA. Pulse shaped DFDMA experiences a lower PAPR with increasing α . Furthermore, the PAPR does not vary with the choice of RU. Pulse shaped LFDMA tends to result in an increased PAPR with increasing α . The PAPR was also shown to vary with the choice of RU. For LFDMA, the time-domain interpolation effect and the phase rotations that result from the choice of RU result in variations in the output mean power after the application of pulse shaping. Hence the resource allocation scheme must take this into account to avoid saturating the RF devices. Overall, in terms of PAPR, DFDMA is shown to be better than LFDMA (with and without pulse shaping). However, in practice it is likely that LFDMA will be easier to implement.

References

[1] L. Cimini Jr., "Analysis and Simulation of a Digital Mobile Channel Using Orthogonal Frequency Division Multiplexing," *IEEE Trans. on Commun*., vol. 33, no. 7, pp. 400-411, July 1985.

[2] R. van Nee and R. Prasad, "*OFDM for Wireless Multimedia Communications*," Artech House, 2000.

[3] D. Falconer, S. L. Ariyavisitakul, A. Benyamin-Seeyar and B. Eidson, "Frequency Domain Equalization for Single-Carrier Broadband Wireless Systems," *IEEE Commun. Mag*., vol. 40, no. 4, pp. 58-66, April 2002.

[4] 3rd Generation Partnership Project (3GPP), "Technical Specification Group Radio Access Network; Physical Layer Aspects for Evolved UTRA," http://www.3gpp.org/ftp/Specs/html-info/25814.htm, Sep 2006.

[5] U. Sorger, I. De Broeck and M. Schnell, "Interleaved FDMA – A New Spread-Spectrum Multiple-Access Scheme," in *Proc. of the IEEE ICC*, vol. 2, pp. 1013-1017, June 1998.

[6] D. Galda and H. Rohling, "A Low-Complexity Transmitter Structure for OFDM-FDMA Uplink Systems," in *Proc. of the IEEE VTC*, vol. 4, pp. 1737-1741, May 2002.

[7] R. Dinis, D. Falconer, C. T. Lam and M. Sabbaghian, "A Multiple Access Scheme for the Uplink of Broadband Wireless Systems," in *Proc. of the IEEE Globecom*, vol. 6, pp. 3803-3812, Nov. 2004.

[8] A. M. Tonello, N. Laurenti and S. Pupolin, "Analysis of the Uplink of an Asynchronous Multi-user DMT OFDMA System Impaired by Time Offsets, Frequency Offsets and Multi-path Fading," in *Proc. of the IEEE VTC*, vol. 3, pp. 1094-1099, Oct. 2000.

[9] H. G. Myung, J. Lim and D. J. Goodman, "Peak-to-Average Power Ratio of Single Carrier FDMA Signals with Pulse Shaping," in *Proc. of the IEEE PIMRC*, pp. 1-5, Sep. 2006.

[10] H. G. Myung, J. Lim and D. J. Goodman, "Single Carrier FDMA for Uplink Wireless Transmission," *IEEE Vehicular Technology Mag*., vol. 1, pp.30-38, Sep. 2006.